Building and Environment, Volume 60, February 2013, Pages 137-149

CFD simulation of wind-induced pressure coefficients on buildings with and without balconies: validation and sensitivity analysis

H. Montazeri*, B. Blocken

Building Physics and Services, Eindhoven University of Technology, P.O. box 513, 5600 MB Eindhoven, The Netherlands

Graphical abstract

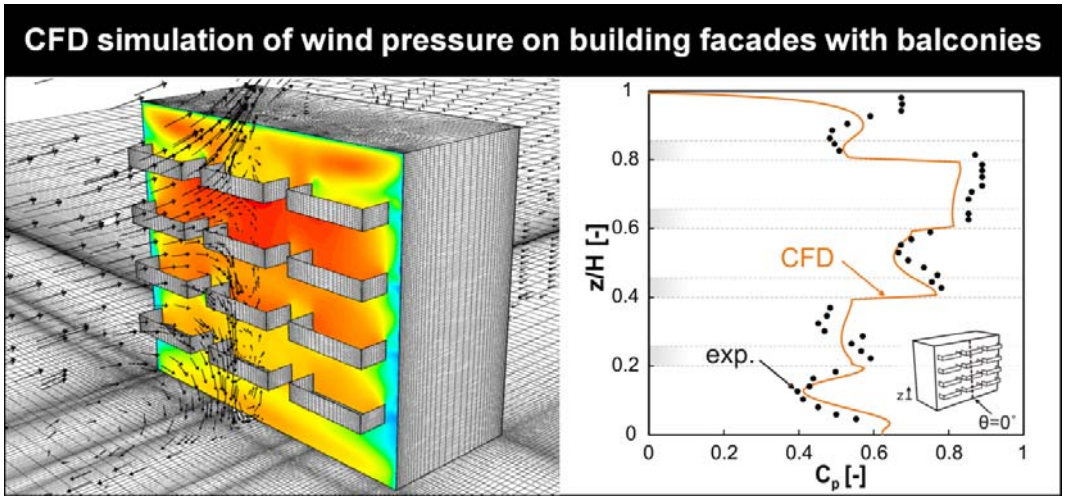

Research highlights:

- Steady 3D RANS CFD simulations for wind pressures on buildings with balconies
- Detailed grid-sensitivity analysis and validation with wind tunnel measurements
- Building balconies strongly influence mean wind pressures at building facades
- Local differences in mean wind pressure coefficients: increase of 0.6, decrease of 0.7
- 3D steady RANS gives very accurate results: 10-15% accuracy at windward facade.

* **Corresponding author:** Hamid Montazeri, Building Physics and Services, Eindhoven University of Technology, P.O. box 513, 5600 MB Eindhoven, the Netherlands. Tel: +31 (0)40 247 5790, Fax: +31 (0)40 243 8595.
E-mail address: h.montazeri@tue.nl

Building and Environment, Volume 60, February 2013, Pages 137-149

CFD simulation of wind-induced pressure coefficients on buildings with and without balconies: validation and sensitivity analysis

H. Montazeri*, B. Blocken

Building Physics and Services, Eindhoven University of Technology, P.O. box 513, 5600 MB Eindhoven, The Netherlands

Abstract

Knowledge of the pressure distribution on building walls is important for the evaluation of wind loads and natural ventilation. Wind-induced pressure distributions are influenced by a wide range of factors including approach-flow conditions, urban surroundings and building geometry. Computational Fluid Dynamics (CFD) can be a valuable tool for determining mean wind pressure coefficients on building facades. However, while many CFD studies of mean wind pressure on buildings have been performed in the past, the vast majority of these studies focused on simple building geometries without facade details such as balconies. These details however can drastically influence the flow pattern and the overall pressure distribution on the facade. This paper presents a systematic evaluation of 3D steady Reynolds-Averaged Navier-Stokes (RANS) CFD for predicting mean wind pressure distributions on windward and leeward surfaces of a medium-rise building with and without balconies. The evaluation is based on a grid-sensitivity analysis and on validation with wind-tunnel measurements. It is shown that building balconies can lead to very strong changes in wind pressure distribution, because they introduce multiple areas of flow separation and recirculation across the facade. The results show that steady RANS, in spite of its limitations, can accurately reproduce the mean wind pressure distribution across the windward facade of the building. The average deviations from the wind-tunnel measurements are 12% and 10% for the building with and without balconies, respectively. In addition, also the important impact of the reference static pressure and the turbulence model are demonstrated.

Keywords: Computational Fluid Dynamics (CFD); building aerodynamics; wind pressure coefficient; sensitivity study; verification and validation

1. Introduction

Knowledge of the pressure distribution on building walls is essential to evaluate wind-induced natural ventilation and to assess wind loads on building walls and building components (e.g. [1-8]). As an example, Building Energy Simulation (BES) programs require pressure coefficient data as input for analysing ventilation and infiltration flow rates [2]. Similarly, design standards need data with a high accuracy for effective-cost designs and reduction of wind damage and cost to building components [9-10].

The pressure distribution on building walls is influenced by a wide range of factors including approach-flow conditions [11-13], urban surroundings [14], building geometry [1] and wind direction [15]. In particular, building facade details such as balconies and other protrusions can affect the peak and mean surface pressure distributions on buildings walls and roofs [16-18].

Pressure coefficients can be determined using full-scale on-site measurements [15, 19-26], reduced-scale wind-tunnel measurements [27-32] or numerical simulation with Computational Fluid Dynamics (CFD) [13, 16, 33-37]. Full-scale measurements offer the advantage that the real situation is studied and the full complexity of the problem is taken into account. However, full-scale measurements are usually only performed in a limited number of points in space. In addition, there is no or only limited control over the boundary conditions [38]. Reduced-scale wind-tunnel measurements allow a strong degree of control over the boundary conditions, however at the expense of – sometimes incompatible – similarity requirements. Furthermore, wind-tunnel measurements are usually also only performed in a limited set of points in space [13]. CFD on the other hand provides whole-flow field data, i.e. data on the relevant parameters in all points of the computational domain [5,39-40]. Unlike wind-tunnel testing, CFD does

* **Corresponding author:** Hamid Montazeri, Building Physics and Services, Eindhoven University of Technology, P.O. box 513, 5600 MB Eindhoven, the Netherlands. Tel: +31 (0)40 247 5790, Fax: +31 (0)40 243 8595.
E-mail address: h.montazeri@tue.nl

not suffer from potentially incompatible similarity requirements because simulations can be conducted at full scale. CFD simulations easily allow parametric studies to evaluate alternative design configurations, especially when the different configurations are all a priori embedded within the same computational domain and grid (see e.g. [41]). CFD is increasingly used to study a wide range of atmospheric and environmental processes. Examples are pedestrian wind comfort and wind safety around buildings [40, 42-46], natural ventilation of buildings [5, 41, 47-53], air pollutant dispersion [54-58], convective heat transfer [59-61], etc. In some of these studies, CFD was applied and evaluated in detail, including verification, validation and sensitivity analyses. CFD has also been used on many occasions in the past to determine mean wind-induced pressure distributions on building facades. However, the vast majority of these studies focused on relatively simple building shapes and plane, smooth facades without protrusions or recessions (e.g. [34-36, 62-63]). Nevertheless, many historical and contemporary building facades are characterised by protrusions and recessions. To the best of our knowledge, a detailed evaluation of steady Reynolds-averaged Navier-Stokes (RANS) CFD has not yet been performed for mean wind pressure distributions on such building facades.

This paper therefore presents a systematic and detailed evaluation of 3D steady RANS CFD for predicting mean wind pressure distributions on building facades with and without balconies for both normal and obliquely approach-flow conditions. The evaluation is based on a grid-sensitivity analysis and on validation with wind-tunnel measurements by Chand et al. [17]. The impact of several computational parameters is also investigated, including the resolution of the computational grid, the reference static pressure and the turbulence model.

In section 2, the wind tunnel experiments by Chand et al. [17] are briefly outlined. Section 3 presents the computational settings and parameters for the reference case, and the validation of the CFD results with the wind-tunnel measurements. In section 4, the sensitivity analysis is performed, including the influence of building balconies on the wind pressure distribution . A discussion on the limitations of the study is given in Section 5. The main conclusions are presented in Section 6.

2. Description of wind tunnel experiments

Atmospheric boundary layer wind-tunnel measurements of wind-induced surface pressure on the facades of a medium-rise building were conducted by Chand et al. [17]. The open-circuit wind tunnel was 14 m long and had a test section of 2.5×1.8 m^2. The atmospheric boundary layer was generated by a combination of three devices: vortex generators, a grid of horizontal rods and a set of roughness elements on the floor of the test section. The resulting vertical profile of mean wind speed at the location of the building (but without building model present) is represented by a log law with aerodynamic roughness length $z_0 = 0.008$ m (model scale, corresponding to 0.24 m in full scale) and a friction velocity $u^*_{ABL} = 0.73$ m/s. The measured incident longitudinal turbulence intensity ranges from 13% near ground level to about 3% at gradient height. Because these profiles were measured at the (virtual) location of the building, they represent the incident, rather than the approach-flow conditions. Using the incident-flow conditions in CFD is important for simulation accuracy [64]. The upstream wind velocity, measured at building height, was equal to 7.1 m/s, yielding a building Reynolds number of 250,000 which is well above the critical value of 11,000 for Reynolds number independent flow [65].

The building at scale 1:30 had dimensions width$\times$depth $\times$height = $0.60 \times 0.25 \times 0.50$ m^3 (reduced scale, see Fig. 1) corresponding to full-scale dimensions $18 \times 7.5 \times 15$ m^3, resulting in a blockage ratio of about 6.6%. To evaluate the effect of building balconies on the mean pressure coefficient, measurements were carried out for a building with and without balconies. Three balconies with width 0.15 m, depth 0.05 m and height 0.03 m were positioned at every one of the five floors, except the ground floor (Fig. 1).

Mean surface pressures were measured along three vertical lines on the windward and leeward facade. Each measurement line was positioned in the middle of the balconies and 45 holes were drilled at equidistant points along it (Fig. 1). In the reminder of this paper, we will refer to these vertical lines as “edge lines” and “centre line”. The measurements were performed with a scanning valve and a digital micro-manometer. Upstream static and dynamic pressures were measured with a Pitot tube mounted 0.90 m upstream of the model and at building height. During the surface pressure measurements, the static tube was connected to the negative port of the scanning valve. So, the manometer indicated the pressure differences of surface pressure and free stream static pressure. The results of the wind-tunnel measurements will be shown together with the validation in the next sections.

3. CFD simulations: reference case

A reference case is defined as a starting point for the sensitivity analysis. It includes a fixed choice for the computational geometry and grid, boundary conditions and turbulence model, as outlined below.

3.1. Computational geometry and grid

A computational model was made of the reduced-scale building model used in the wind-tunnel measurements. The dimensions of the computational domain were chosen based on the best practice guidelines by Franke et al. [66] and Tominaga et al. [67]. The upstream domain length is 5H = 2.5 m. The resulting dimensions of the domain were $W \times D \times H = 10.6 \times 10.25 \times 3$ m^3, which corresponds to $318 \times 307.5 \times 90$ m^3 in full scale. The computational grid was created using the surface-grid extrusion technique presented by van Hooff and Blocken [41]. The procedure was executed with the aid of the pre-processor Gambit 2.4.6, resulting in a hybrid grid with 2,102,250 prismatic and hexahedral cells. The grid is shown in Figs. 2a-c. 20 and 10 cells are used along the width and depth of the balconies, respectively, as shown in Fig. 2c. A maximum stretching ratio of 1.2 controls the cells located in the immediate surroundings of the building model. The grid resolution resulted from a grid-sensitivity analysis that will be outlined in Section 4.1. The minimum and maximum cell volumes in the domain are approximately 5×10^{-8} m³ and 7.5×10^{-2} m³, respectively. The distance from the centre point of the wall adjacent cell to the wall, for the windward, leeward and ground plane is 0.0017m, 0.0022m and 0.0025m, respectively. This corresponds to y* values between 20 and 350. As standard wall functions are used in this study, these values ensure that the centre point of the wall-adjacent cell is placed in the logarithmic layer. The domain shape (Fig. 2a) allows modelling different wind directions (0° and 45°, corresponding to the experiments).

3.2. Boundary conditions

For wind direction θ = 0°, plane 1 in Figure 2a is the inlet plane, plane 3 the outlet plane and planes 2 and 4 are the side planes. In the simulations the inlet boundary conditions (mean velocity U, turbulent kinetic energy k and turbulence dissipation rate ε were based on the measured incident vertical profiles of mean wind speed U and longitudinal turbulence intensity I_u (Fig. 3) The turbulent kinetic energy k was calculated from U and I_u using Eq. (1), where a is a parameter in the range between 0.5 and 1.5 [50]. In this study, as recommended by Tominaga et al. [67], a=1 is chosen. The turbulence dissipation rate ε is given by Eq. (2), with κ the von Karman constant (= 0.42).

$$k(z) = a\left(I_u(z)u(z)\right)^2 \tag{1}$$

$$\varepsilon(z) = \frac{u_{ABL}^{*3}}{\kappa(z + z_0)} \tag{2}$$

For the ground surface, the standard wall functions by Launder and Spalding [68] with roughness modification by Cebeci and Bradshaw [69] are used. The values of the roughness parameters, i.e. the sand-grain roughness height k_s (m) and the roughness constant C_s, were determined using their consistency relationship with the aerodynamic roughness length z_0 derived by Blocken et al. [70]. For Fluent 6.3, this relationship is:

$$k_s = \frac{9.793 z_0}{C_s} \tag{3}$$

Given the upstream domain length of 5H, the roughness parameters are taken to reproduce the roughness of the wind-tunnel turntable, which is considered to be smooth and for which z_0 = 0.0018 m is assumed. The selected (reduced-scale) values according to Eq. (3) are k_s=0.0025 m and C_s=7.0. Standard wall functions are also used at the building surfaces, but with zero roughness height k_s=0 (C_s=0.5). Zero static pressure is applied at the outlet plane. Symmetry conditions, i.e. zero normal velocity and zero normal gradients of all variables, are applied at the top and lateral sides of the domain. As recommended by Blocken et al. [70-72], the absence of unintended streamwise gradients (i.e. horizontal inhomogeneity) in the vertical profiles of mean wind speed and the turbulence parameters was confirmed by performing simulations in an empty domain (i.e. without building present).

3.3. Solver settings

The commercial CFD code Fluent 6.3.26 was used to perform the simulations. The 3D steady RANS equations were solved in combination with the realizable k−ε turbulence model by Shih et al. [73]. The SIMPLE algorithm was used for pressure-velocity coupling, pressure interpolation was second order and second-order discretization schemes were used for both the convection terms and the viscous terms of the governing equations. Convergence was assumed to obtain when all the scaled residuals levelled off and reached a minimum of 10^{-6} for x, y momentum, 10^{-5} for y momentum and 10^{-4} for k, ε and continuity.

3.4. Results and comparison with wind tunnel experiments

The CFD results for the reference case are compared with the wind-tunnel measurements by Chand et al. [17]. The pressure coefficients are computed as $C_p = (P-P_0)/(0.5\rho U_{ref}^2)$ where P is the pressure at the surface, P_0 the reference static pressure, $\rho = 1.225$ kg/m³ the air density and U_{ref} is the reference wind speed at building height ($U_{ref} = 7.1$ m/s at $z = 0.5$ m). Fig. 4 provides the CFD results of static pressure along a vertical line 0.9 m upstream of the building, where the Pitot tube for the reference static pressure was mounted in the experiment. It can be seen that the static pressure at building height is about 4.3 Pa. Note that Chand et al. [17] did not report the static pressure that they used to calculate the C_P values. In the present study, we used the value of 4.3 Pa for this purpose.

Fig. 5 compares the CFD results and the wind-tunnel results of C_P along the vertical measurement lines at the facade (shown in Fig. 1) for the case with balconies. The general agreement is quite good. For the lines at the windward facade (Fig. 5a and 5b), the average absolute deviation between CFD results and measurements is 0.052 and 0.072 for the edge lines and centre line, respectively. In particular the vertical C_P gradients (increase and decrease of C_P along these vertical lines) due to the presence of the balconies are quite well reproduced. Note that there are some discrepancies especially at the lower half of the facade at edge lines, where CFD overestimates C_P, and at the upper half of the facade at the centre line, where CFD provides underestimations. The exact reasons for this are not clear, but it is possible that the expected acceleration of the flow over the smooth turntable of the wind tunnel, directly upstream of the building model, has had some effect on the measurement values. Overall, in spite of the well-known deficiences of steady RANS CFD to reproduce separating and recirculating flow [67, 74], the agreement between the CFD and the wind-tunnel results is considered to be good. Also at the leeward facade, the agreement is quite good (Fig. 5c and 5d). The average absolute deviation between CFD results and measurements is 0.069 and 0.070 for the edge lines and centre line, respectively. Note that there is a systematic underestimation of the absolute value of C_P by CFD at the leeward facade.

4. CFD simulations: sensitivity analysis

To analyse the sensitivity of the results to various geometrical and computational parameters, systematic changes are made to the reference case that was outlined in the previous section. In every section, one of the geometrical or computational parameters is varied, while all others are kept identical to those in the reference case.

4.1. Impact of computational grid resolution

Performing a grid-sensitivity analysis is important to reduce the discretisation errors and the computational time. In this study, a grid-sensitivity analysis was performed based on two additional grids; a coarser grid and a finer grid. Coarsening and refining was performed with an overall linear factor $\sqrt{2}$. As mentioned before, the basic mesh had 2,102,250 cells. The coarse grid had 720,937 cells, while the fine grid had 6,755,370 cells. The three grids are shown in Fig. 6. The results for C_P on the three grids are compared in Fig. 7, indicating only a very limited dependence of the results on the grid resolution. The average absolute deviation between the CFD results and the measurements for the edge lines is 0.056, 0.052 and 0.052 for the coarse, basic and fine grid, respectively. For the centre line, the average absolute deviations are 0.068, 0.072 and 0.073. A small deviation is between the coarse grid and basic grid for the upper part of the building, and between fine grid and basic grid for the space between the third and fourth floors. Negligible grid sensitivity is found for the other parts. Therefore, the basic grid is retained for further analysis.

4.2. Impact of reference static pressure

As mentioned before, the actual value of the reference static pressure in the wind tunnel is not known, as it was not reported in the paper by Chand et al. [17]. The paper does mention that it was measured by a Pitot tube placed 0.9 m upstream of the building and at building height. In the present paper, the CFD result of the static pressure at this position of the Pitot tube was used as the reference static pressure (see subsection 3.4). In the wind-tunnel experiments, it was assumed that the presence of the model had no influence on the measurement of upstream static pressure at this position. However, the simulation results (see Fig. 4) showed that the model affects the upstream flow causing an increase in static pressure. To illustrate the importance of a correct reference value for this static pressure, Figure 8 shows the results obtained with $P_{ref} = 1$, 3, 5 and 7 Pa. For the edge lines, the average absolute deviations between the CFD results and the measurements are 0.165, 0.103, 0.052 and 0.051, for 1, 3, 5 and 7 Pa, respectively. For the centre line, these deviations are 0.122, 0.076, 0.072 and 0.099. These results show that a small change in the upstream static pressure can lead to very large deviations in C_P. This implies that accurate values for this reference static pressure are crucial for a successful CFD validation effort. For CFD validation purposes, it is important that the position of P_{ref} is the same as in the experiments. In

general, a reference position that is outside the wind-flow pattern disturbed by the building model should be used.

4.3. Impact of turbulence model

3D steady RANS simulations were made in combination with five turbulence models: (1) the standard k−ε model (Sk−ε) [75]; (2) the realizable k−ε model (Rk−ε) [73]; (3) the renormalization Group k−ε model (RNG k−ε) [76-77]; (4) the standard k−ω model (Sk−ω) [78] and (5) the Reynolds Stress Model (RSM) [79]. For the standard k−ω model, the inlet vertical profile for ω is determined from that of k and ε using Eq. (4), where C_μ is a constant equal to 0.09. For the RSM model, the Reynolds stress components are obtained from the turbulent kinetic energy k assuming isotropy of turbulence (see Eq. (5)):

$$\omega(z) = \frac{\varepsilon(z)}{C_\mu \, k(z)} \tag{4}$$

$$\begin{aligned} \overline{u_i'^2} &= \frac{2}{3}k \qquad (i = 1,2,3) \\ \overline{u_i' u_j'} &= 0.0 \end{aligned} \tag{5}$$

The results are shown in Figure 9. The average absolute deviations for the edge lines and centre line for each turbulence model are given in Table 1. The differences between the models are most pronounced near ground level, where the RNG k-ε model tends to overestimate the pressure variations. The standard k−ω model generally provides a slight overestimate of the pressure, while the results of the RSM are very close to those of the standard and realizable k-ε model (reference case).

4.4. Impact of building balconies for perpendicular approach flow

The impact of building balconies on C_P is investigated by comparing simulations for buildings with and without balconies. This subsection presents the results for perpendicular approach flow. The results are displayed in Figure 5, 10, 11 and 12. The following observations are made:

- Figure 10 compares the simulated and measured C_p along the edge lines and centre line for the facade without balconies. For both the windward and the leeward facade, a good to very good agreement with the measurements is obtained. The main deviations are again found at the lower half of the facade. The average absolute deviations in Figures 10a, 10b, 10c and 10d are 0.045, 0.046, 0.039 and 0.055, respectively.
- Comparing Figures 5 and 10 clearly shows the very large impact of the building balconies on the C_p distribution. The presence of the balconies yields a very different C_P profile along the height of the building facade, with a succession of lower and higher pressure zones, caused by the multitude of flow separation and recirculation areas induced by the balconies.
- Figure 11 compares the simulated distribution of C_p across the entire windward facade for the case with and without balconies. This figure confirms the much larger complexity of the C_P distribution across the facade with balconies. In particular:
  1) For the second and third row of balconies, the presence of these balconies generally leads to an increase in C_P. The reason is the direct impingement of the flow onto these balconies and onto the facade behind them, yielding a large stagnation area. To some extent, the balconies act as compartments with a nearly constant pressure. This effect is most pronounced for the third row of balconies, but also present for the second row.
  2) For the first and fourth row of balconies, flow separation and reattachment can lead to local increases and decreases in C_P. Especially for the side balconies, large gradients are observed.
- Figure 12 shows the impact of balconies on the surface-averaged pressure coefficients for each balcony space. The width of the surfaces is equal to the width of each balcony, i.e. 0.15 m. The height of the surfaces is 0.1 m. The surface-averaged C_p values are presented for the two cases: with balconies (Fig. 12a) and without balconies (Fig. 12b). Fig. 12c also shows the relative percentage difference of surface-averaged C_p for the two cases. The results show that the presence of the fourth row of balconies leads to a substantial decrease in the surface-average C_p of about 30%. The third row of balconies, however, is situated closer to the stagnation area and the change in surface-averaged C_p is therefore negligible. For the second and first row of balconies, their presence substantially increases the surface-averaged C_p except for the middle balconies.

4.5. Impact of building balconies for oblique approach-flow

Simulations and measurements were also made for oblique flow (wind direction 45°). The results are provided in Figures 13, 14, 15 and 16. The following observations are made:

- Figures 13a-c compare the simulated and measured C_p along the vertical lines in the middle and at the edges of the windward facade. A good to very good agreement is obtained between the simulations and the measurements. The average absolute deviations in Figures 13a, b and c are 0.028, 0.029 and 0.028, respectively.
- Figures 13d-f compare the simulated and measured C_p for the leeward facade. Here, as opposed to the case with perpendicular flow, the agreement is not good. The average absolute deviations in Figures 13d, e and f are 0.095, 0.155 and 0.068, respectively.
- Figure 14a-c show the results for the windward facade with balconies. The average absolute deviations in Figures 14a, b and c are 0.035, 0.058 and 0.039, respectively.
- Figure 14d-f show the results for the leeward facade with balconies, with averaged absolute deviations of 0.095, 0.156 and 0.068, respectively.
- Overall, a good agreement is obtained, although locally some significant discrepancies are noted. Comparing Figure 13 and 14 again clearly shows the large impact of the building balconies on the C_p distribution.
- Figure 15 finally compares the simulated distribution of C_p across the entire windward facade for the case with and without balconies. The complexity of the distribution is directly attributable to multiple areas of flow separation, recirculation and reattachment on the windward building facade.
- Figure 16 shows the results on the surface-averaged pressure coefficients. The results show that the impact of balconies for oblique flow is much more complex than for perpendicular flow.

5. Discussion

It is important to mention the three main limitations of this study.

(1) The study only considered steady RANS CFD simulations, as the purpose was to investigate how well steady RANS CFD would be able to reproduce wind pressure distributions across building facades, especially for facades with balconies. In spite of the well-known deficiencies of steady RANS, a good agreement was obtained between CFD simulations and wind-tunnel measurements, both for the windward facade without balconies and for the windward facade with balconies. Also for the leeward facade and for perpendicular wind, a good agreement was obtained. However, larger deviations were obtained for wind pressures on the leeward facade for oblique wind. Obtaining a better agreement here would necessitate the use of Large Eddy Simulation (LES), which however is much more computationally expensive than steady RANS.

(2) Only an isolated medium-rise building was considered. Further work should assess the accuracy of steady RANS to reproduce the effect of balconies on pressure distributions on high-rise buildings, and on buildings surrounded by other buildings.

(3) The explicit focus of the study was the assessment of steady RANS CFD for a given building geometry with given balcony geometries. Future work could focus on optimal balcony design. In order to optimize the arrangement of balconies, a parametric analysis needs to be performed. This optimization should be done by taking the impact of different factors into account such as building geometry, position, dimension and number of balconies, etc. Besides the impact of balconies on the surface pressure distribution of the building, to achieve an optimum arrangement of balconies, wind comfort and wind safety assessment also need to be studied.

In spite of these limitations, the present study has analysed the possibilities and limitations of steady RANS for assessing the effect of balconies on wind-induced pressure coefficients. It has also investigated the effect of the balconies on these coefficients by comparing simulations for buildings with and without balconies. Finally, also a detailed sensitivity study has been performed, including the most important computational parameters such as computational grid, turbulence model, approach-flow mean velocity profile and wind direction. Note that the focus of this paper was explicitly on the pressure distribution across the building facade. Further studies could include analysis of the static pressure distribution in the area around the building (i.e. not at the building façade) and of the wind-velocity pattern.

6. Conclusions

This paper has presented a systematic evaluation of 3D steady RANS CFD for the prediction of the mean wind pressure distribution on windward and leeward surfaces of a medium-rise building with and without balconies. The evaluation is based on a grid-sensitivity analysis and on validation with wind-tunnel measurements. The study was motivated by the lack of knowledge on the accuracy and reliability of CFD for determining mean wind pressure coefficients on building facades with balconies. Although indeed many CFD studies of mean wind pressure distributions on buildings have been performed in the past, the vast majority of these studies focused on simple building geometries without facade details such as balconies. These details however are important because they can drastically change the flow pattern

and the overall pressure distribution on the facade. In addition, many historical and contemporary building facades are characterised by protrusions and recessions.

The present study has shown that 3D steady RANS CFD, in spite of its limitations, is suitable to predict the wind-induced mean pressures at windward building facades with (and without) balconies. It has also been shown that the presence of building balconies can indeed lead to very strong changes in wind pressure distribution on these windward facades, because the balconies introduce multiple areas of flow separation, recirculation and reattachment. 3D steady RANS CFD has also been shown to provide accurate predictions of the mean wind pressure at the leeward wall in case of a perpendicular approach flow wind direction. This however is not the case for oblique flow, where large discrepancies with the wind-tunnel measurements have been found. Finally, also the impact of the turbulence model, the reference static pressure and the wind direction have been investigated, and it has been shown that a careful selection of these parameters is very important for accurate and reliable results.

References

[1] Uematsu Y, Isyumov N. Wind pressures acting on low-rise buildings. J Wind Eng Ind Aerodyn 1999;82:1-25.

[2] Cóstola D, Blocken B, Hensen JLM. Overview of pressure coefficient data in building energy simulation and airflow network programs. Build Environ 2009;44:2027-36.

[3] Montazeri H, Azizian R. Experimental study on natural ventilation performance of one-sided wind catcher. Build Environ 2008;43:2193-202.

[4] Montazeri H, Montazeri F, Azizian R, Mostafavi S. Two-sided wind catcher performance evaluation using experimental, numerical and analytical modeling. Renew Energy 2010;35:1424-35.

[5] Chen Q. Ventilation performance prediction for buildings: A method overview and recent applications. Build Environ 2009;44:848-58.

[6] Linden PF. The fluid mechanics of natural ventilation. Annu Rev Fluid Mech 1999;31:201-38.

[7] Hunt GR, Linden PP. The fluid mechanics of natural ventilation—displacement ventilation by buoyancy-driven flows assisted by wind. Build Environ 1999;34:707-20.

[8] Karava P, Stathopoulos T, Athienitis AK. Wind driven flow through openings – A review of discharge coefficients. Int J Vent 2004;3:255-66.

[9] Ginger JD, Letchford CW. Net pressures on a low-rise full-scale building. J Wind Eng Ind Aerodyn 1999;83:239-50.

[10] Chen X, Zhou N. Equivalent static wind loads on low-rise buildings based on full-scale pressure measurements. Eng Struct 2007;29:2563-75.

[11] Letchford CW, Mehta KC. The distribution and correlation of fluctuating pressures on the Texas Tech Building. J Wind Eng Ind Aerodyn 1993;50:225-34.

[12] Wu F, Sarkar PP, Mehta KC, Zhao Z. Influence of incident wind turbulence on pressure fluctuations near flat-roof corners. J Wind Eng Ind Aerodyn 2001;89:403-20.

[13] Stathopoulos T. Computational wind engineering: Past achievements and future challenges. J Wind Eng Ind Aerodyn 1997;67–68:509-32.

[14] Kim YC, Yoshida A, Tamura Y. Characteristics of surface wind pressures on low-rise building located among large group of surrounding buildings. Eng Struct 2012;35:18-28.

[15] Levitan ML, Mehta KC, Vann WP, Holmes JD. Field measurements of pressures on the Texas tech building. J Wind Eng Ind Aerodyn 1991;38:227-34.

[16] Stathopoulos T, Zhu X. Wind pressures on building with appurtenances. J Wind Eng Ind Aerodyn 1988;31:265-81.

[17] Chand I, Bhargava PK, Krishak NLV. Effect of balconies on ventilation inducing aeromotive force on low-rise buildings. Build Environ 1998;33:385-96.

[18] Maruta E, Kanda M, Sato J. Effects on surface roughness for wind pressure on glass and cladding of buildings. J Wind Eng Ind Aerodyn 1998;74–76:651-63.

[19] Levitan ML, Mehta KC. Texas Tech field experiments for wind loads part 1: building and pressure measuring system. J Wind Eng Ind Aerodyn 1992;43:1565-76.

[20] Maruyama T, Taniguchi T, Okazaki M, Taniike Y. Field experiment measuring the approaching flows and pressures on a 2.4m cube. J Wind Eng Ind Aerodyn 2008;96:1084-91.

[21] Richardson GM, Robertson AP, Hoxey RP, Surry D. Full-scale and model investigations of pressures on an industrial/agricultural building. J Wind Eng Ind Aerodyn 1990;36, Part 2:1053-62.

[22] Richards PJ, Hoxey RP. Pressures on a cubic building—Part 1: Full-scale results. J Wind Eng Ind Aerodyn 2012;102:72-86.

[23] Richards PJ, Hoxey RP. Wind loads on the roof of a 6m cube. J Wind Eng Ind Aerodyn 2008;96:984-93.

[24] Richards PJ, Hoxey RP, Short LJ. Wind pressures on a 6m cube. J Wind Eng Ind Aerodyn 2001;89:1553-64.

[25] Snæbjörnsson JT, Geurts CPW. Modelling surface pressure fluctuations on medium-rise buildings. J Wind Eng Ind Aerodyn 2006;94:845-58.

[26] Caracoglia L, Jones NP. Analysis of full-scale wind and pressure measurements on a low-rise building. J Wind Eng Ind Aerodyn 2009;97:157-73.
[27] Castro IP, Robins AG. The flow around a surface-mounted cube in uniform and turbulent streams. J Fluid Mech 1977;79:307-35
[28] Cochran LS, Cermak JE. Full- and model-scale cladding pressures on the Texas Tech University experimental building. J Wind Eng Ind Aerodyn 1992;43:1589-600.
[29] Richards PJ, Hoxey RP, Connell BD, Lander DP. Wind-tunnel modelling of the Silsoe Cube. J Wind Eng Ind Aerodyn 2007;95:1384-99.
[30] Surry D. Pressure measurements on the Texas tech building: Wind-tunnel measurements and comparisons with full scale. J Wind Eng Ind Aerodyn 1991;38:235-47.
[31] Richardson GM, Surry D. The Silsoe structures building: Comparison between full-scale and wind-tunnel data. J Wind Eng Ind Aerodyn 1994;51:157-76.
[32] Stathopoulos T, Saathoff P. Wind pressure on roofs of various geometries. J Wind Eng Ind Aerodyn 1991;38:273-84.
[33] Murakami S, Mochida A, Hibi K. Three-dimensional numerical simulation of air flow around a cubic model by means of large eddy simulation. J Wind Eng Ind Aerodyn 1987;25:291-305.
[34] Murakami S, Mochida A. 3-D numerical simulation of airflow around a cubic model by means of the k-ϵ model. Journal of Wind Engineering and Industrial Aerodynamics 1988;31:283-303.
[35] Baetke F, Werner H, Wengle H. Numerical simulation of turbulent flow over surface-mounted obstacles with sharp edges and corners. J Wind Eng Ind Aerodyn 1990;35:129-47.
[36] Mochida A, Murakami S, Shoji M, Ishida Y. Numerical Simulation of flowfield around Texas Tech Building by Large Eddy Simulation. J Wind Eng Ind Aerodyn 1993;46–47:455-60.
[37] Nore K, Blocken B, Thue JV. On CFD simulation of wind-induced airflow in narrow ventilated facade cavities: Coupled and decoupled simulations and modelling limitations. Build Environ 2010;45:1834-46.
[38] Reinhold T. Wind tunnel modeling for civil engineering applications. Cambridge: Cambridge University Press; 1982.
[39] Blocken B, Gualtieri C. Ten iterative steps for model development and evaluation applied to Computational Fluid Dynamics for Environmental Fluid Mechanics. Environ Modell Softw 2012;33:1-22.
[40] Blocken B, Janssen WD, van Hooff T. CFD simulation for pedestrian wind comfort and wind safety in urban areas: General decision framework and case study for the Eindhoven University campus. Environ Modell Softw 2012;30:15-34.
[41] van Hooff T, Blocken B. Coupled urban wind flow and indoor natural ventilation modelling on a high-resolution grid: A case study for the Amsterdam ArenA stadium. Environ Modell Softw 2010;25:51-65.
[42] Blocken B, Persoon J. Pedestrian wind comfort around a large football stadium in an urban environment: CFD simulation, validation and application of the new Dutch wind nuisance standard. J Wind Eng Ind Aerodyn 2009;97:255-70.
[43] He J, Song CCS. Evaluation of pedestrian winds in urban area by numerical approach. J Wind Eng Ind Aerodyn 1999;81:295-309.
[44] Richards PJ, Mallinson GD, McMillan D, Li YF. Pedestrian level wind speeds in downtown Auckland. Wind Struct 2002;5:151-64.
[45] Hirsch C, Bouffioux V, Wilquem F. CFD simulation of the impact of new buildings on wind comfort in an urban area. Workshop Proceedings, Cost Action C14, Impact of Wind and Storm on City Life and Built Environment. Nantes, France2002.
[46] Yoshie R, Mochida A, Tominaga Y, Kataoka H, Harimoto K, Nozu T, et al. Cooperative project for CFD prediction of pedestrian wind environment in the Architectural Institute of Japan. J Wind Eng Ind Aerodyn 2007;95:1551-78.
[47] Evola G, Popov V. Computational analysis of wind driven natural ventilation in buildings. Energy Build 2006;38:491-501.
[48] Jiang Y, Chen Q. Effect of fluctuating wind direction on cross natural ventilation in buildings from large eddy simulation. Build Environ 2002;37:379-86.
[49] van Hooff T, Blocken B, Aanen L, Bronsema B. A venturi-shaped roof for wind-induced natural ventilation of buildings: Wind tunnel and CFD evaluation of different design configurations. Build Environ 2011;46:1797-807.
[50] Norton T, Grant J, Fallon R, Sun D-W. Optimising the ventilation configuration of naturally ventilated livestock buildings for improved indoor environmental homogeneity. Build Environ 2010;45:983-95.
[51] Ramponi R, Blocken B. CFD simulation of cross-ventilation for a generic isolated building: Impact of computational parameters. Build Environ 2012;53:34-48.
[52] Kato S, Murakami S, Mochida A, Akabayashi S-i, Tominaga Y. Velocity-pressure field of cross ventilation with open windows analyzed by wind tunnel and numerical simulation. J Wind Eng Ind Aerodyn 1992;44:2575-86.

[53] Heiselberg P, Li Y, Andersen A, Bjerre M, Chen Z. Experimental and CFD evidence of multiple solutions in a naturally ventilated building. Indoor Air 2004;14:43-54.
[54] Blocken B, Stathopoulos T, Saathoff P, Wang X. Numerical evaluation of pollutant dispersion in the built environment: Comparisons between models and experiments. J Wind Eng Ind Aerodyn 2008;96:1817-31.
[55] Gousseau P, Blocken B, Stathopoulos T, van Heijst GJF. CFD simulation of near-field pollutant dispersion on a high-resolution grid: A case study by LES and RANS for a building group in downtown Montreal. Atmos Environ 2011;45:428-38.
[56] Hanna SR, Brown MJ, Camelli FE, Chan ST, Coirier WJ, Hansen OR, et al. Detailed simulations of atmospheric flow and dispersion in downtown Manhattan: An applications of five computational fluid dynamics models. Bull Amer Meteor Soc 2006;87:1713-26.
[57] Tominaga Y, Stathopoulos T. CFD modeling of pollution dispersion in a street canyon: Comparison between LES and RANS. J Wind Eng Ind Aerodyn 2011;99:340-8.
[58] Tominaga Y, Stathopoulos T. Numerical simulation of dispersion around an isolated cubic building: Model evaluation of RANS and LES. Build Environ 2010;45:2231-9.
[59] Blocken B, Defraeye T, Derome D, Carmeliet J. High-resolution CFD simulations for forced convective heat transfer coefficients at the facade of a low-rise building. Build Environ 2009;44:2396-412.
[60] Karava P, Jubayer CM, Savory E. Numerical modelling of forced convective heat transfer from the inclined windward roof of an isolated low-rise building with application to photovoltaic/thermal systems. Appl Therm Eng 2011;31:1950-63.
[61] Saneinejad S, Moonen P, Defraeye T, Carmeliet J. Analysis of convective heat and mass transfer at the vertical walls of a street canyon. J Wind Eng Ind Aerodyn 2011;99:424-33.
[62] Delaunay D, Lakehal D, Pierrat D. Numerical approach for wind loads prediction on buildings and structures. J Wind Eng Ind Aerodyn 1995;57:307-21.
[63] Panneer Selvam R. Computation of pressures on Texas Tech University building using large eddy simulation. J Wind Eng Ind Aerodyn 1997;67–68:647-57.
[64] Blocken B, Stathopoulos T, Carmeliet J. Wind environmental conditions in passages between two long narrow perpendicular buildings. J Aerospace Eng - ASCE 2008;21:280-7.
[65] Snyder WH. Guideline for fluid modeling of atmospheric diffusion. U.S. Environmental Protection Agency Report No. EPA-600/8-81-0091981.
[66] Franke J, Hellsten A, Schlünzen H, Carissimo B. Best practice guideline for the CFD simulation of flows in the urban environment. Brussels: COST Office 2007.
[67] Tominaga Y, Mochida A, Yoshie R, Kataoka H, Nozu T, Yoshikawa M, et al. AIJ guidelines for practical applications of CFD to pedestrian wind environment around buildings. J Wind Eng Ind Aerodyn 2008;96:1749-61.
[68] Launder BE, Spalding DB. The numerical computation of turbulent flows. Comput Methods Appl Mech Eng 1974;3:269–89.
[69] Cebeci T, Bradshaw P. Momentum transfer in boundary layers. New York: Hemisphere Publishing Corp; 1977.
[70] Blocken B, Stathopoulos T, Carmeliet J. CFD simulation of the atmospheric boundary layer: wall function problems. Atmos Environ 2007;41:238-52.
[71] Blocken B, Moonen P, Stathopoulos T, Carmeliet J. Numerical study on the existence of the venturi effect in passages between perpendicular buildings. J Eng Mech - ASCE 2008;134:1021-8.
[72] Blocken B, Carmeliet J, Stathopoulos T. CFD evaluation of wind speed conditions in passages between parallel buildings—effect of wall-function roughness modifications for the atmospheric boundary layer flow. J Wind Eng Ind Aerodyn 2007;95:941-62.
[73] Shih T-H, Liou WW, Shabbir A, Yang Z, Zhu J. A new k-ϵ eddy viscosity model for high reynolds number turbulent flows. Comput Fluids 1995;24:227-38.
[74] Murakami S. Comparison of various turbulence models applied to a bluff body. J Wind Eng Ind Aerodyn 1993;46–47:21-36.
[75] Jones WP, Launder BE. The prediction of laminarization with a two-equation model of turbulence. Int J Heat Mass Transfer 1972;15:301-14.
[76] Yakhot V, Orszag SA, Thangam S, Gatski TB, Speziale CG. Development of turbulence models for shear flows by a double expansion technique. Physics of Fluids ;4:1510-20.
[77] Choudhury D. Introduction to the renormalization group method and turbulence modeling: Technical Memorandum TM-107; 1993.
[78] Wilcox DC. Turbulence modeling for CFD: La Canada, California: DCW Industries, Inc.; 1998.
[79] Launder BE, Reece GJ, Rodi W. Progress in the development of a Reynolds-stress turbulence closure. J Fluid Mech 1975;68:537-66

FIGURES

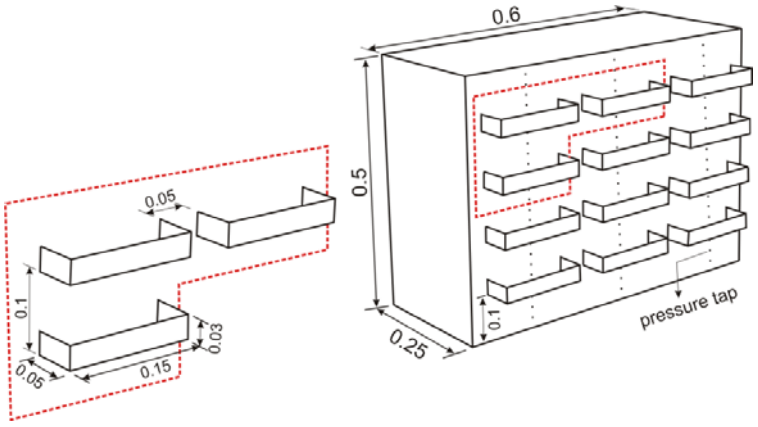

Figure 1. Geometry of building model and balconies (dimensions in meter at model scale).

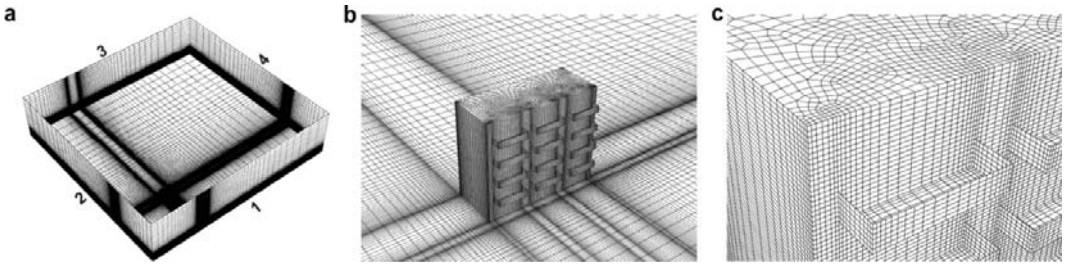

Figure 2. Computational grid. (a) Grid at bottom and side faces of computational domain. (b) Grid at building surfaces and ground surface. (c) Detail of grid near balconies.

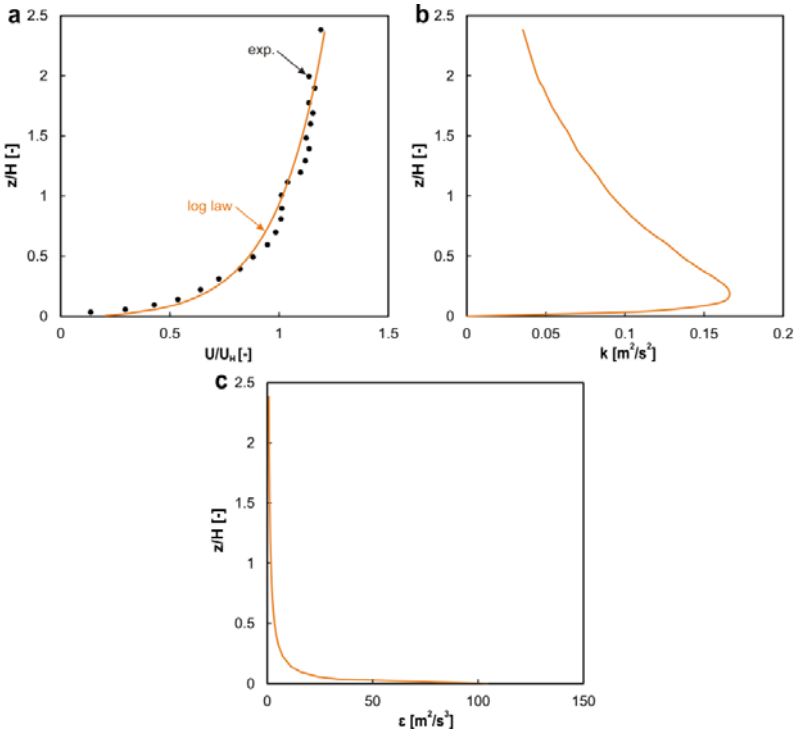

Figure 3. (a) Measured profile (dotted line) and fitted log law profile (solid line) of ratio of mean wind speed U to mean wind speed U_H at building height. Inlet vertical profile of (b) turbulent kinetic energy k and (c) turbulence dissipation rate ε.

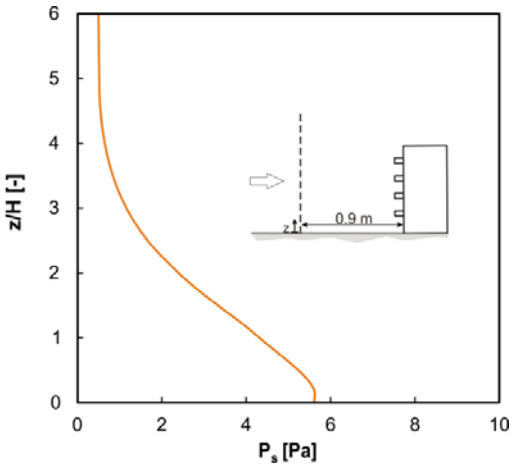

Figure 4. Simulated vertical profile of static pressure upstream of the building.

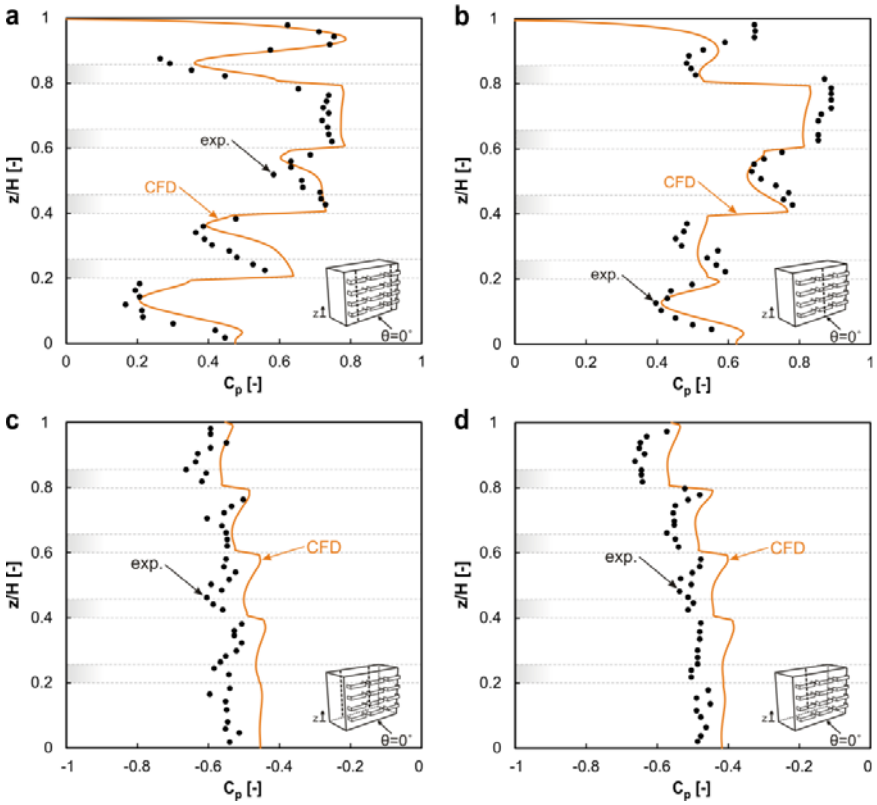

Figure 5. Comparison of pressure coefficient C_P by CFD simulation results and wind-tunnel experiments along (a) edge lines on windward facade; (b) centre line on windward facade; (c) edge lines on leeward facade; (d) centre line on leeward facade.

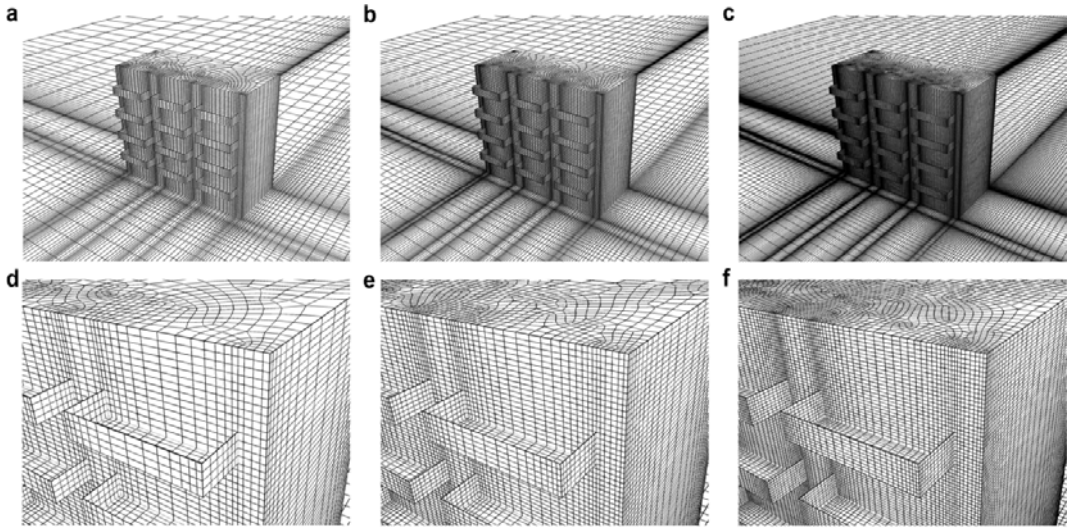

Figure 6. Computational grids for grid-sensitivity analysis. (a) coarse grid; (b) basic grid; (c) fine grid.

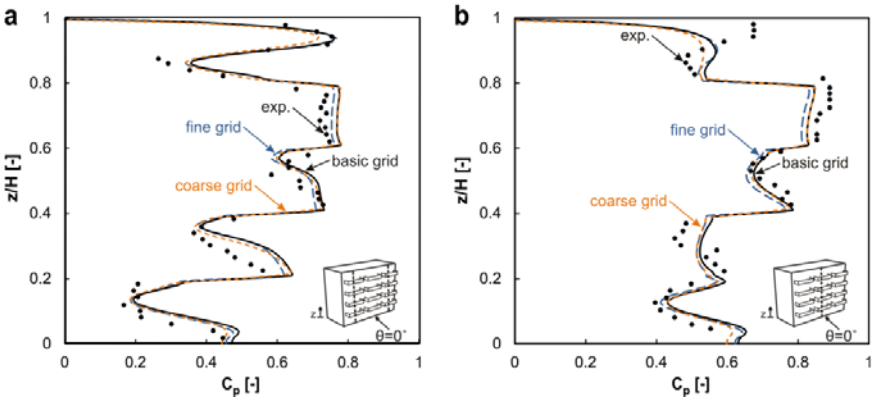

Figure 7. Results for grid-sensitivity analysis: pressure coefficient C_P values along (a) edge line and (b) centre line for the three grids.

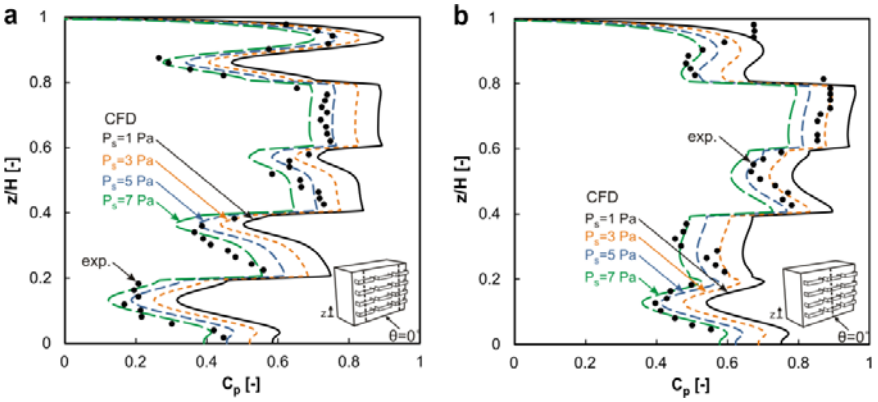

Figure 8. Impact of static reference pressure on CFD simulation results of pressure coefficient C_P along (a) edge line and (b) centre line.

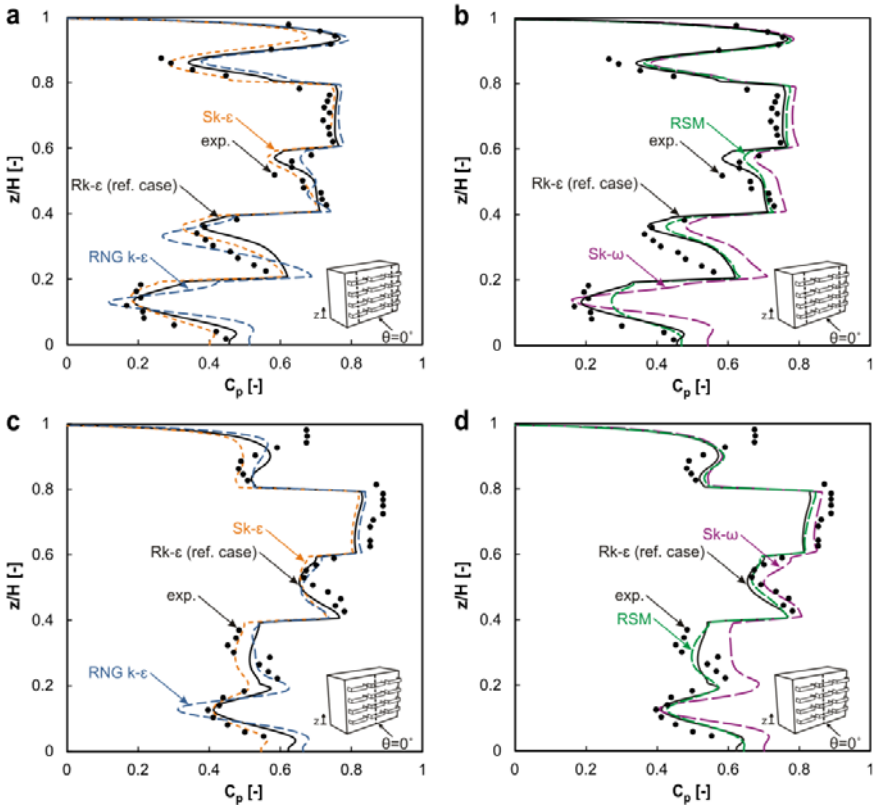

Figure 9. Impact of turbulence model on CFD simulation results of pressure coefficient C_P along (a,b) edge line and (c,d) centre line.

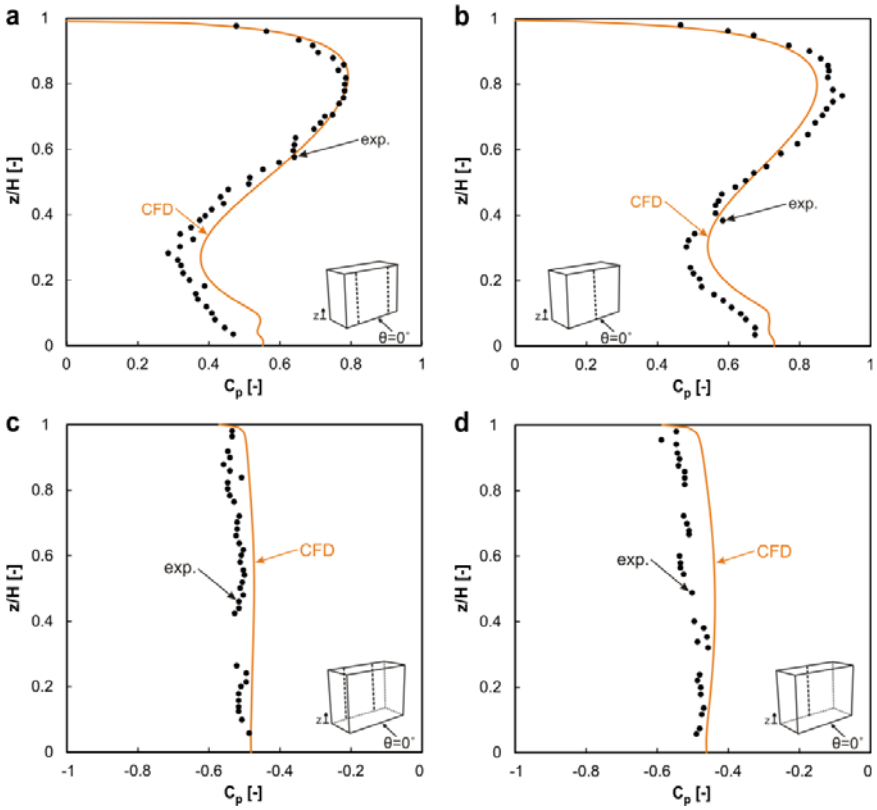

Figure 10. Comparison of pressure coefficient C_P by CFD simulation results and wind-tunnel experiments for building without balconies along (a) edge lines on windward facade; (b) centre line on windward facade; (c) edge lines on leeward facade; (d) centre line on leeward facade.

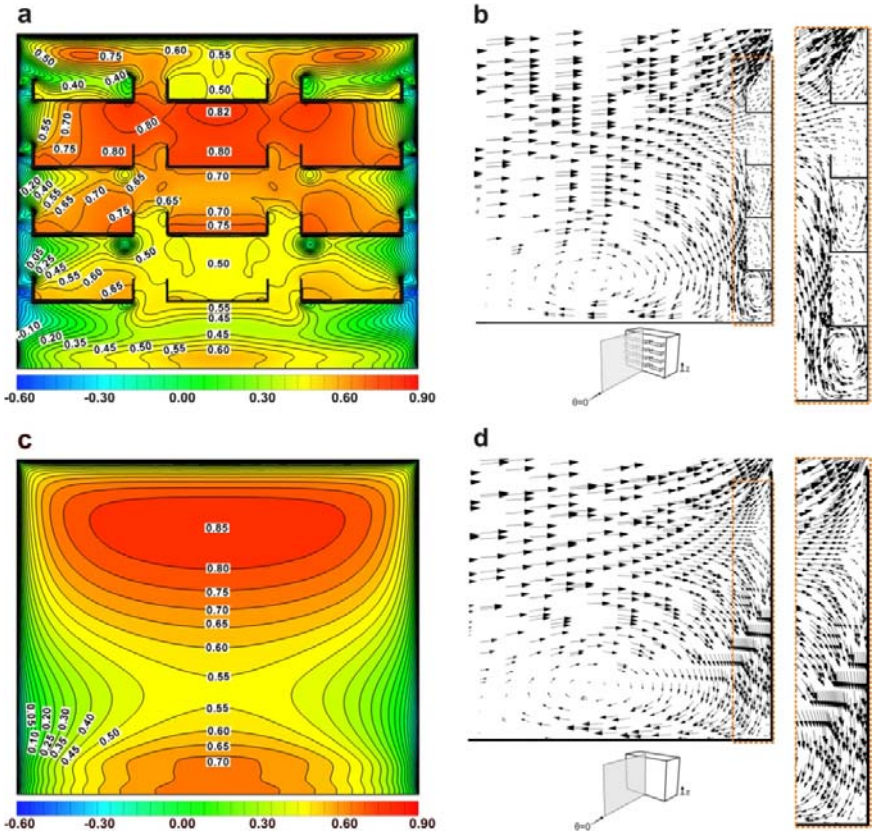

Figure 11. (a) Pressure coefficient C_P distribution across windward facade of building with balconies, for wind direction perpendicular to the windward facade. (b) Velocity vector field in cross-section (centre plane). (c) C_P distribution for building without balconies. (d) Same as (b), but for building without balconies.

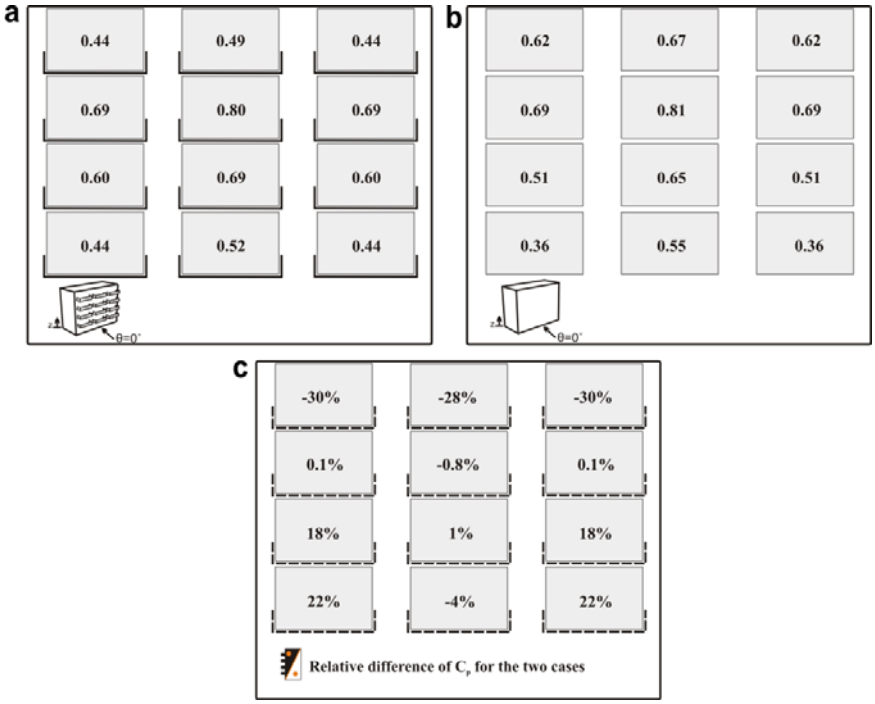

Figure 12. Impact of balconies on the surface-averaged pressure coefficients for each balcony space, for wind direction perpendicular to the windward facade. The surface-averaged C_P for the case (a) with balconies and (b) without balconies. (c) The relative percentage difference of surface-averaged C_p for the two cases.

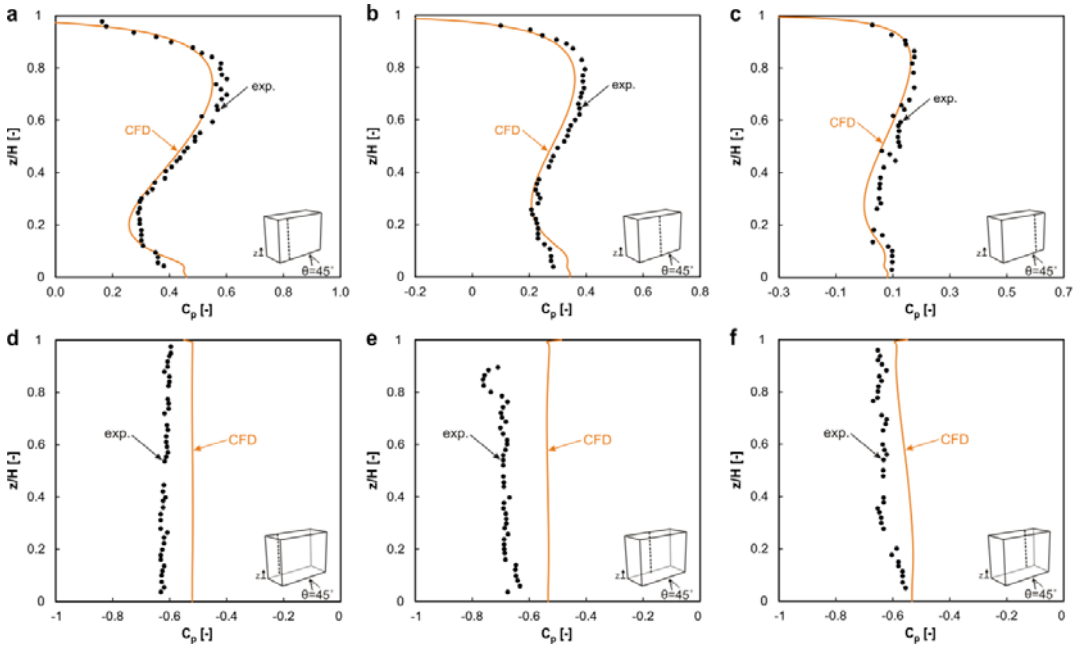

Figure 13. Comparison of pressure coefficient C_P by CFD simulation results and wind-tunnel experiments for building without balconies and for oblique wind direction 45°, along: (a) windward upstream edge line, (b) windward centre line, (c) windward downstream edge line, (d-f) same lines at leeward facade.

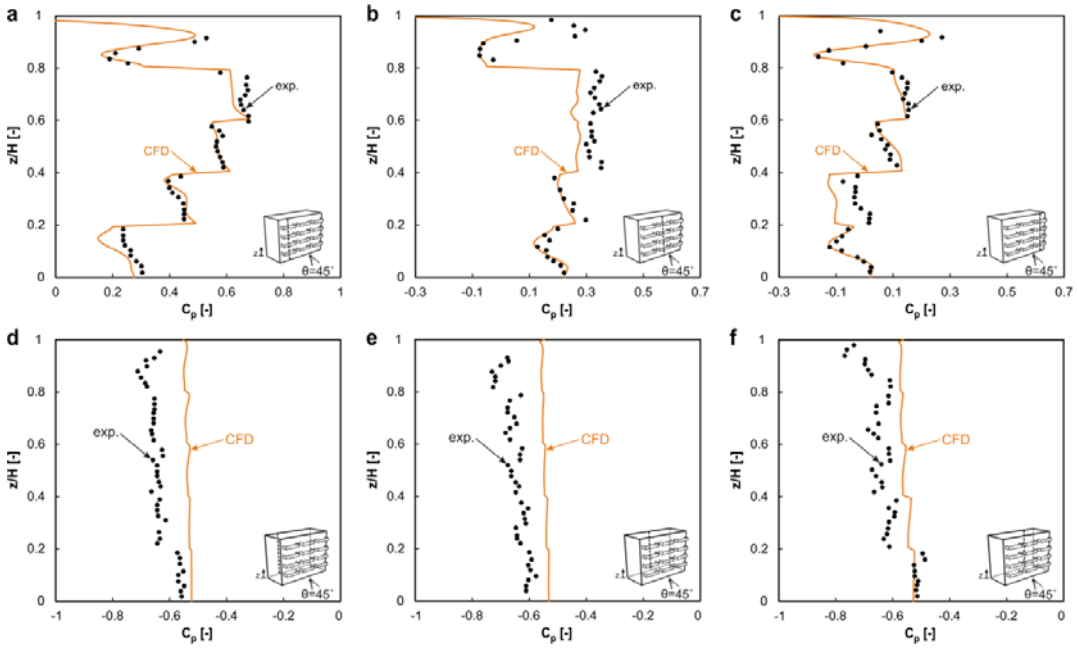

Figure 14. Comparison of pressure coefficient C_P by CFD simulation results and wind-tunnel experiments for building with balconies and for oblique wind direction 45°, along: (a) windward upstream edge line, (b) windward centre line, (c) windward downstream edge line, (d-f) same lines at leeward facade.

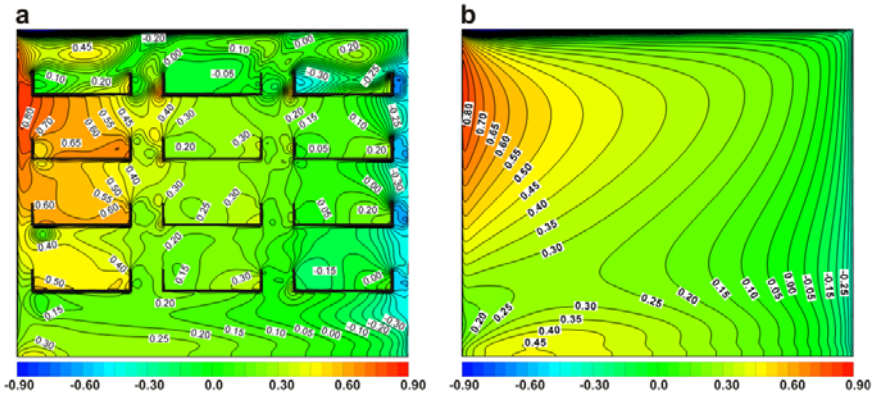

Figure 15. (a) Pressure coefficient C_P distribution across windward facade of building with balconies, for wind direction at 45° to the windward facade. (b) C_P distribution for building without balconies.

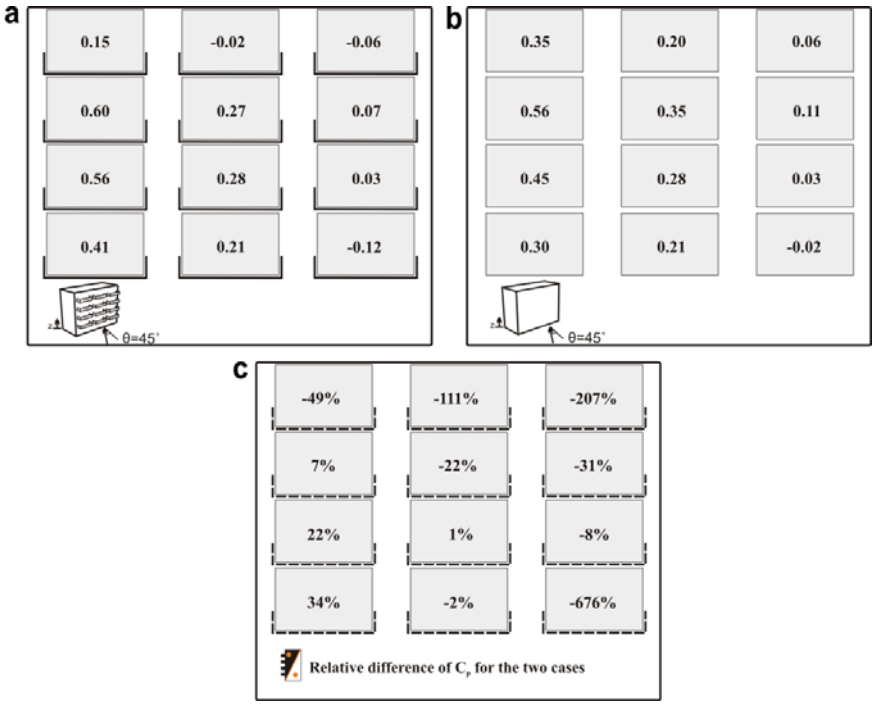

Figure 16. Impact of balconies on the surface-averaged pressure coefficients for each balcony space, for wind direction at 45° to the windward facade. The surface-averaged C_P for the case (a) with balconies and (b) without balconies. (c) The relative percentage difference of surface-averaged C_p for the two cases.

TABLE

Table 1. The average absolute deviations for the edge lines and centre line for each turbulence model

Turbulence model	Edge line	Centre line
Standard k−ε model	0.044	0.071
Realizable k−ε model	0.052	0.072
RNG k−ε model	0.067	0.070
Standard k−ω model	0.098	0.087
Reynolds Stress model	0.064	0.067